Pergamon

Int. J. Heat Mass Transfer. Vol. 38, No. 8, pp. 1443–1455, 1995

0017-9310/95 $9.50+0.00

0017-9310(94)00251-7

Simulation of reaction and transport in catalyst particles with partial external and internal wetting

D. N. JAGUSTE and S. K. BHATIA†

Department of Chemical Engineering, Indian Institute of Technology, Powai, Bombay 400076, India

(*Received* 31 *January* 1994 *and in final form* 27 *July* 1994)

Abstract—Simultaneous heat, mass and momentum transport phenomena accompanying phase transition and exothermic chemical reaction in unsaturated capillary porous media are investigated in this study with respect to a partially externally wetted nonisothermal catalyst pellet. The internal wetting efficiency, on which the effectiveness factor is strongly dependent, is determined by the internal and external transport processes, and is sensitive to the extent of external wetting as well as the degree of saturation of the surrounding gas. Adsorbate and capillary condensate transport, generally ignored for catalytic reactions, can have a dominating influence on the rate of reaction in the vapor-filled region.

INTRODUCTION

Partially filled (unsaturated) porous media occur in a wide variety of fields of scientific and technological interest. In such media transport may occur by diffusion and viscous flow in both liquid and vapor phases, and also by surface diffusion in an adsorbed phase. The literature on the subject is rather extensive, and since this study analyses the effects mainly in partially wetted catalyst particles, such as in trickle bed reactors (TBRs), we focus our attention on the relevant issues in this field. In such reactors, due to liquid maldistribution, the catalyst particles see a variety of wetting environments. In addition to different flow features the catalyst particles in different regions in the bed are wetted by the liquid film to different extents and, as a result, are subjected to different heat and mass transfer conditions. Hence, for better understanding of TBRs, it is necessary to study the performance of particles subjected to each of these environments [1]. However, while some studies exist [2–6] on catalyst particles in the dry region of the trickle bed, most studies are primarily focused [7, 8] on partially externally wetted pellets, internally filled with liquid. A key assumption in these latter studies is that strong capillary forces cause complete filling of the pores by liquid imbibition from the externally wetted surface. Although the pore filling assumption is probably valid for isothermal or endothermic reactions, the assumption may not hold for exothermic reaction systems with volatile reactants and/or gas phase unsaturated in condensable component. Yet several modeling studies of exothermic reaction systems involving volatile liquid reactants have assumed isothermal conditions, or treated the degree of internal wetting as an independent parameter [9–11]. More realistic analyses [4–6, 12], however, consider the interplay between capillary condensation phenomena and thermal effects in predicting the degree of internal wetting. Among these the work of Harold [12] also considers the effect of external wetting, but simplifies the problem by choosing one-dimensional geometry.

The present work addresses several important issues such as two-dimensional formulation, variable external wetting efficiency, pore size distribution, capillary imbibition, capillary condensate and adsorbate transport in the vapor-filled region, and external transport resistances which were never simultaneously considered previously. Various important ideas and findings reported in several earlier studies are reconciled and, while the physical picture chosen pertains to that for a multiphase catalytic reaction, the model is quite general. Indeed, the additional features such as occurrence of (an exothermic) chemical reaction and the partial external wetting, inherent in the single particle studies in trickle bed reactors, add to the complexity and make this problem more generalized than other studies in this area.

PHYSICAL PICTURE

The model single catalyst pellet is depicted in Fig. 1. The two-dimensional slab of lengths L_x and $2L_y$ is wetted on one side by a flowing liquid film, a rivulet, comprised only of the volatile species A. The rest of the pellet is directly exposed to the bulk gas comprised of species A and other noncondensables. This two dimensional geometry and wetting configuration is a simplification of partially wetted spherical or cylindrical pellet, as seen in Fig. 1. The dimensions of the pellet and external wetting efficiency η_{ex} can be varied

† Author to whom correspondence should be addressed.

NOMENCLATURE

a	empirical constant in equation (8)
a_m	molecular area [m^2]
C	$\bar{v}_A P_o / RT_{lo}$
C_{Tg}	total gas phase molar concentration [mol m^{-3}]
C_{Tl}	liquid phase molar concentration [mol m^{-3}]
C'_{Tl}	adsorbed phase concentration [mol m^{-3}]
d_{AK}	$D^\circ_{Am}/D^\circ_{K,A}(r_a)$
D°_{Am}	diffusivity of component A in mixture at bulk temperature [m^2 s^{-1}]
$D^\circ_{K,A}$	Knudsen diffusivity of A at bulk temperature [m^2 s^{-1}]
D^*_{aA}	$D_{aA}/(D^\circ_{Am}\varepsilon_a^2)$
D^*_{iA}	$D_{iA}/(D^\circ_{Am}\varepsilon_a^2)$
D^{s*}_{iA}	$D^s_{iA}/(D^\circ_{Am}\varepsilon_a^2)$
D^{l*}_{iA}	$D^l_{iA}/(D^\circ_{Am}\varepsilon_a^2)$
D_{eA}	effective diffusivity [m^2 s^{-1}]
D^*_{eA}	$D_{eA}/(D^\circ_{Am}\varepsilon_a^2)$
E_A	activation energy [J mol^{-1}]
E_{ff}	effectiveness factor, equation (58)
$f_i(\rho)$	equation (30)
F	$r_a N a_m C_{Tl}/2$
h	empirical constant in equation (8)
h_{gs}	gas–solid heat transfer coefficient [W m^{-2} K^{-1}]
h_{ls}	liquid–solid heat transfer coefficient [W m^{-2} K^{-1}]
H_l	$\varepsilon_a^2 r_a^2 P_o C_{Tl} C_{Pl}/8\mu_l K_{el}$
ΔH_r	heat of reaction [J mol^{-1}]
k_r	reaction rate constant [mol$^{(1-n)}$ m$^{3(n-1)}$ s^{-1}]
K_{eg}	effective thermal conductivity in gas-filled region [W m^{-1} K^{-1}]
K_{el}	effective thermal conductivity in liquid-filled region [W m^{-1} K^{-1}]
K_{gs}	gas–solid mass transfer coefficient [m s^{-1}]
K_p	intrinsic permeability for laminar flow [m^2]
K^*_{Pig}	$8K_{Pig}/\bar{r}_i^2\varepsilon_i$
K^*_{Pil}	$8K_{Pil}/\bar{r}_i^2\varepsilon_i$
L	L_x/L_y
L_x	length of the slab along X direction [m]
L_y	half the length of slab along Y direction [m]
n	order of reaction with respect to A
M_l	$C_{Tl} r_a^2 P_o/8\mu_l D^\circ_{Am} C_{Tgo}$
NU_{gs}	$h_{gs} L_x/K_{el}$
NU_{ls}	$h_{ls} L_x/K_{el}$
P_g	gas phase pressure inside the pellet [Pa]
P_o	bulk gas phase pressure [Pa]
P_c	capillary suction pressure [Pa], equation (9)
P^*_C	P_c/P_o
P_{Ao}	vapor pressure of component A at temperature T_{lo} [Pa]
P^*_{Ao}	P_{Ao}/P_o
P_l	liquid phase pressure in region L [Pa]
P_{ll}	liquid phase pressure in region LL [Pa]
P^*_l	P_l/P_o
P^*_{ll}	P_{ll}/P_o
Q	K_{eg}/K_{el}
r	pore radius [m]
r_1, r_2	principal radii of curvature [m]
r_C	critical pore radius [m]
r_{cp}	equation (6) [m]
$\bar{r}_i$	mean micropore radius [m]
r_M	mean radius of curvature of the meniscus [m]
r_a	mean macropore radius [m]
R	universal gas constant [J mol^{-1} K^{-1}]
S	surface area per unit particle volume [m^{-1}]
S^*_{ig}	$S_{ig}\bar{r}_i/2\varepsilon_i$
SH	$K_{gs} L_x/\varepsilon_a^2 D^\circ_{Am}$
T	T_{go}/T_{lo}
T_g	temperature in region G
T_{go}	bulk gas phase temperature [K]
T_l	temperature in region L
T_{ll}	temperature in region LL
T_{lo}	bulk liquid phase temperature [K]
$\bar{v}_A$	partial molar volume of component A [m^3 mol^{-1}]
V	$C_{Tl} r_a^2 \varepsilon_a^2 P_o \lambda_A/8\mu_l K_{el} T_{lo}$
W_A	λ_A/RT_{lo}
W_s	a/RT_{go}
X	abscissa in physical coordinate system [m]
x	X/L_x
x_g	equation (61)
x_l	equation (62)
x_{ll}	equation (63)
Y	ordinate in physical coordinate system [m]
y	Y/L_y
y_A	mole fraction of condensable species A.

Greek symbols

α	equation (49)
β	$[-\Delta H_r] D^\circ_{Am} \varepsilon_a^2 C_{Tgo}/K_{eg} T_{go}$
Δ	X coordinate of interfacial point [m]
δ	Δ/L_x
ε_i	microporosity
ε_a	macroporosity
ϕ_o	$[L_x^2 k_r(T_{go}) C_{Tgo}^{n-1}/D^\circ_{Am}\varepsilon_a^2]^{1/2}$
Γ	length of external liquid film in X direction [m]
γ	Γ/L_x
η_{ex}	external wetting efficiency
η_i	internal wetting efficiency
θ	angle between tangent to the interface and the X axis [rad]
θ_c	contact angle [rad]

$\hat{\theta}$	equilibrium contact angle [rad]
θ_g	T_g/T_{go}
θ_l	T_l/T_{lo}
θ_{ll}	T_{ll}/T_{lo}
Θ	number of molecular layers in adsorbed phase
Θ^*	$\Theta/F\bar{p}_i$
λ_A	latent heat of vaporization of pure A [J mol^{-1}]
μ_l	viscosity of liquid [Pa s]
ν	E_A/RT_{go}
ρ	r/r_a
ρ_c	r_c/r_a
ρ_{cp}	r_{cp}/r_a
$\bar{\rho}_i$	$\bar{r}_i/r_a$
σ	surface tension [N m^{-1}]
σ_i	standard deviation in micropore distribution
Ψ	$L_x-\Gamma-\Delta(1)$, thickness of region L on pellet surface
ψ	Ψ/L_x.

Superscripts

*	dimensionless quantity
l	liquid phase
s	surface phase.

Subscripts

A	condensable component A
a	macropore
g	gas phase
go	bulk gas phase
i	micropore
ig	gas-filled portion of the microparticle
il	liquid-filled portion of the microparticle
l	liquid phase
lo	bulk liquid phase
o	bulk condition.

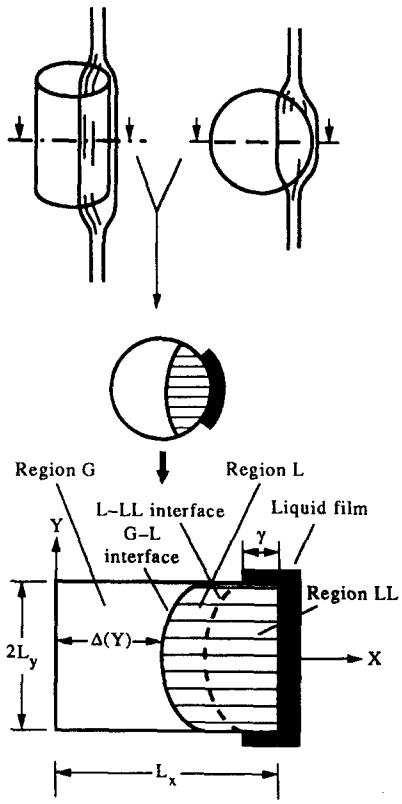

Fig. 1. Model catalyst pellet.

by adjusting L_x, L_y and the dimensionless rivulet width γ.

The catalyst particle is considered to comprise of compressed microporous microparticles. All pores are assumed to be of cylindrical shape, and while the intraparticle micropores are ascribed a size distribution, the interparticle macropores are considered to be of uniform size. Since the macropores form a continuous network, the gas-filled region is considered to be one in which all the macropores are filled with vapor. Thus, the interface separates the comp etely liquid-filled portion from the region in which all the macropores are vapor-filled. However, due to capillary condensation some of the micropores in the microparticles surrounded by gas would be liquid-filled. Although, surface diffusion may not be important in catalysis at elevated temperatures (involving only gases), it is known to be of considerable importance in the low temperature reaction of a condensable vapor, as in the catalytic dehydration of ethanol [13]. Thus, surface diffusion and capillary condensate transport as subsequently discussed, can significantly alter the overall permeability of the microparticles.

For the wetting configuration described above, for certain conditions, the pellet may be completely or almost completely filled and the interface may reside at the corner of the pellet. For simplicity we focus only on those conditions for which the interface is in the interior of the pellet, away from the $X = 0$ face of the pellet.

THEORETICAL CONSIDERATIONS

Vapor–liquid equilibrium

The vapor–liquid equilibrium and the mechanism of condensation and evaporation in cylindrical capillaries is well understood [14, 15], and is given by the generalized Kelvin equation across a curved interface:

$$\frac{y_i P_g}{x_i P_i^o} = \exp\left[-\frac{2\sigma\bar{v}_i}{R_g T_g r_M}\right] \quad (1)$$

in which r_M is the mean radius of curvature, expressed as

$$\frac{2}{r_M} = \left[\frac{1}{r_1} + \frac{1}{r_2}\right] \tag{2}$$

where r_1 and r_2 are the principal radii of curvature. During capillary condensation in a cylindrical pore, the vapor–liquid interface is known to pass through a series of unstable configurations before the final stable hemispherical shape is attained. However, at the two extreme situations, namely, evaporation of liquid from a liquid-filled pore and inception of condensation in a vapor-filled pore, the meniscus takes hemispherical and cylindrical shapes, respectively [14]. The mean radius of curvature r_M for these two cases is readily related to the radius (r) of the cylindrical pore. Thus, for a cylindrical meniscus, for which $r_1 = r$ and $r_2 = \infty$ one obtains $r_M = 2r$. For a hemispherical shaped meniscus, r_M can be related to r by

$$r_M = \frac{r}{\cos(\theta_c)} \tag{3}$$

where θ_c is the contact angle, which may be different from the equilibrium property $\hat{\theta}$, when the meniscus is at the pore-mouth. Consequently, for the perfect hemisphere, for which $\theta_c = 0$ and $r_1 = r_2 = r$, one obtains $r_M = r$. Thus, although the vapor–liquid equilibrium in a porous body is uniquely defined with respect to the curvature of the meniscus, it is not so with respect to the pore radius.

In a partially internally wetted particle having a continuous pore size distribution, depending on temperature and partial pressure of condensable components, pores having radii smaller than a particular value called critical pore radius are filled with the condensed liquid. Although, the curvatures of the liquid menisci are the same in all liquid-filled pores (in agreement with the generalized Kelvin equation), the largest liquid-filled pores (of critical pore radius) are on the verge of emptying, with contact angle $\hat{\theta}$, during evaporation process or are just liquid-filled during condensation process. Hence, the curvature of menisci in the porous solid, during the process of evaporation and condensation can be related to the critical pore radius r_C. Thus, for evaporation, substituting $r_M = r_C/\cos(\hat{\theta})$ in the generalized Kelvin equation [equation (1)], we obtain

$$\frac{y_i P_g}{x_i P_i^o} = \exp\left[-\frac{2\sigma \bar{v}_i \cos(\hat{\theta})}{R_g T_g r_c}\right] \tag{4}$$

which is referred to, in this work, as the Kelvin equation. For condensation, which is initiated with cylindrical meniscus, substituting $r_M = 2r_c$ in equation (1), yields the modified Cohan equation

$$\frac{y_i P_g}{x_i P_i^o} = \exp\left[-\frac{\sigma \bar{v}_i}{R_g T_g r_c}\right]. \tag{5}$$

Accounting for the presence of adsorbed layer the actual critical pore radius r_{cp} could be related to r_c in equations (4) and (5) by

$$r_{cp} = r_c + t \tag{6}$$

in which t is the thickness of the adsorbed layer. Assuming that the adsorbed layer has liquid-like density, the thickness t may be written as

$$t = \frac{\Theta}{a_m N C_{Tl}} \tag{7}$$

where Θ is the number of molecular layers in adsorbed phase, a_m is the molecular area and C_{Tl} the liquid phase molar concentration of the adsorbate component. Θ in equation (7) may be related to the partial pressure of condensable component in bulk gas phase by a Frenkel–Halse–Hill equation for multilayer adsorption [16]:

$$\ln\left[\frac{P_A(T_g)}{P_A^o(T_g)}\right] = -\frac{a}{RT_g\Theta^h} \tag{8}$$

in which a and h are empirical constants.

Capillary suction pressure

A curved liquid–vapor interface not only reduces the saturation vapor pressure but also presents a capillary suction pressure at the interface, due to the action of surface tension at the meniscus, causing imbibition of liquid from the external liquid film, which is at higher pressure, and capillary condensate transport due to the gradient in capillary suction pressure. This capillary suction pressure can be calculated from the Laplace equation [15]

$$P_c = \frac{2\sigma\cos(\hat{\theta})}{r_c}. \tag{9}$$

Transport of condensable component in vapor-filled region

Adsorbate flow in microparticle. There are three possible ways in which a condensable (or an adsorbable) vapor can flow though a microporous medium: gas phase and surface flow through vapor-filled pores and capillary condensate flow through liquid-filled pores. However in the range of pressures where capillary condensation occurs, surface flow and capillary condensate flow usually dominate over bulk vapor flow [17].

The simultaneous transport in the coexisting surface and capillary condensed phases is represented here by a modified hydrodynamic model [18]. In the model, both the surface and the capillary condensate flow are separately treated like viscous flow through a capillary. While the flow in surface phase is represented by Flood's hydrodynamic model [19], the capillary condensate flow is considered to obey Darcy's law. The resulting transport coefficients D_{iA}^l and D_{iA}^s for the flow in liquid-filled pores and in surface phase, respectively, are given [18] by

$$D^{l}_{iA} = \frac{K_{Pil} R T_g C^{2}_{Tl}}{\mu_l y_A C_{Tg}} \quad (10)$$

and

$$D^{s}_{iA} = \frac{K_{Pig} R T_g C'^{2}_{Tl}}{\mu_l y_A C_{Tg}} \quad (11)$$

in which K_{Pil} and K_{Pig} are the local average intrinsic permeabilities for laminar flow in liquid-filled region and gas-filled region, respectively, and C'_{Tl} is the adsorbed phase concentration, expressed as moles per unit volume of pore space. The effective microparticle diffusivity D_{iA} is thus given by

$$D_{iA} = D^{l}_{iA} + D^{s}_{iA} \quad (12)$$

Effective diffusivity in vapor-filled region. While gas phase diffusion on the pellet scale generally occurs predominantly through the macroporous structure, because of the relatively small size of the micropores, the flux of condensable components in the microstructure may be considerably enhanced because of capillary condensate transport and surface diffusion [19, 20]. Since the transport resistance of the point contacts is generally relatively large, Maxwell's equation offers a convenient means of modeling the overall transport of condensable species A. While developed [21] for the case of a dilute suspension of spheres, the equation has been found to be applicable for a broad range of void fractions [22]. In the present analysis, we consider the microparticle effectiveness factor to be unity, and adopt Maxwell's model for obtaining the effective diffusivity D_{eA} of condensable component A:

$$D_{eA} = D_{aA} \times \left\{ \frac{2/D_{iA} + 1/D_{aA} - 2(1-\varepsilon_a)(1/D_{iA} - 1/D_{aA})}{2/D_{iA} + 1/D_{aA} + (1-\varepsilon_a)(1/D_{iA} - 1/D_{aA})} \right\}. \quad (13)$$

In equation (13) ε_a is the macroporosity, and D_{aA} is the macropore diffusivity expressed as

$$D_{aA} = \varepsilon_a (1/D_{Am} + 1/D_{K,A}(r_a))^{-1} \quad (14)$$

in which D_{Am} is the bulk mixture diffusivity and $D_{K,A}(r_a)$ is the Knudsen diffusivity in a macropore of radius r_a, and macropore tortuosity is taken as $1/\varepsilon_a$.

MATHEMATICAL MODEL

In this work we consider an exothermic reaction, effectively of the type A → products, in which A is the liquid phase reactant and the products are noncondensable. Also, we assume that the reaction in the gas-filled portion of the partially internally wetted catalyst pellet dominates the overall reaction rate, and the reaction rate in the liquid-filled region is negligible in comparison. An example of such reaction system is the catalytic decomposition of hydrazine [23]. Alternatively, the reaction can also be considered to be of the type A(l) + B(g) → products, in which the noncondensable reactant B is sparingly soluble in the liquid phase, and is the limiting reactant in the liquid-filled portion. This latter reaction system is supported by at least two experimental studies, that of Sedriks and Kenney [9] on the hydrogenation of crotonaldehyde on a palladium-supported catalyst, and of Satterfield and Ozel [24] on the hydrogenation of benzene, where the direct vapor phase reaction dominated even when the extent of internal wetting was large. For simplicity, it is further assumed that the reaction in the vapor-filled region is pseudo nth order with respect to the condensable species A, and that the products of reaction are noncondensable.

The other important assumptions involved in modeling are as follows:

(1) Micropore effectiveness factor is unity everywhere in both the capillary-condensed liquid and vapor phases.

(2) Intraparticle transport in liquid-filled portion is dominated by capillary imbibition.

(3) Gas phase transport is dominated by diffusion and the gaseous transport is sufficiently rapid to prevent a pressure build up in the gas filled pores.

(4) Reaction rate is controlled by surface reaction and is the same in liquid-filled pores as in the surrounding vapor-filled pores.

(5) Contribution of convective heat transfer in gas phase is considered negligible as compared to conduction.

(6) Intraparticle liquid velocity is assumed to be linearly related to the pressure gradient according to Darcy's law.

(7) Macropores are of uniform size and all the pores in the pellet are of cylindrical shape.

Since the wetting configuration of the slab is symmetric about the X axis (Fig. 1) we consider only the upper half, for the mathematical analysis. For computational purposes the actual physical space of the pellet is divided into three distinct regions: the gas-filled region (region G), a liquid-filled region, the external boundaries of which are directly exposed to the bulk gas phase (region L), and a liquid-filled region, the external boundaries of which are covered by the flowing liquid film (region LL). Further, the fictitious L–LL interface, separating region L and LL, is assumed to be parallel to the gas–liquid interface (G–L interface). In what follows we present the dimensionless mathematical model for each of these regions.

The gas-filled region: region G$(0 < x < \delta(y);\ 0 < y < 1)$

The diffusion equation for reactant A is given by

$$\frac{\partial}{\partial x}\left(\frac{D^{*}_{eA}}{\theta_g}\frac{\partial y_A}{\partial x}\right) + L^2 \frac{\partial}{\partial y}\left(\frac{D^{*}_{eA}}{\theta_g}\frac{\partial y_A}{\partial y}\right) = \phi_0^2 \left(\frac{y_A}{\theta_g}\right)^{n} \exp\left(\frac{\nu[\theta_g - 1]}{\theta_g}\right). \quad (15)$$

The dimensionless effective diffusivity D^*_{eA} in this equation is obtained as discussed in the preceding section. The dimensionless macropore diffusivity, D^*_{aA}, and the microparticle diffusivity, D^*_{iA}, of component A are expressed as follows:

$$D^*_{aA} = \frac{1}{\varepsilon_a}\left(\frac{1}{\theta_g^{1.75}} + \frac{d_{AK}}{\theta_g^{0.5}}\right)^{-1} \tag{16}$$

$$D^*_{iA} = D^{s*}_{iA} + D^{l*}_{iA}, \tag{17}$$

where D^{s*}_{iA} and D^{l*}_{iA} represent, respectively, the dimensionless diffusivities for the adsorbate and capillary condensate transport of species A in the microparticles, and are given by the following equations

$$D^{s*}_{iA} = \frac{M_l \theta_g^2 \bar{\rho}_i^2 \varepsilon_i^3 K^*_{Pig}}{\varepsilon_a^2 C y_A}\left(\frac{\Theta^* S^*_{ig}}{\varepsilon_{ig}}\right)^2 \tag{18}$$

$$D^{l*}_{iA} = \frac{M_l \theta_g^2 \bar{\rho}_i^2 \varepsilon_i K^*_{Pil}}{\varepsilon_a^2 C y_A} \tag{19}$$

in which

$$\varepsilon_{ig} = \varepsilon_i - \varepsilon_{il} \tag{20}$$

$$\varepsilon_{il} = \int_0^{\rho_{cp}} f_i(\rho)\, d\rho \tag{21}$$

$$\rho_{cp} = \rho_c + \frac{\bar{\rho}_i \Theta^*}{2} \tag{22}$$

$$\rho_c = \frac{P^*_c C}{T}\left\{\theta_g \ln\left(\frac{P^*_{Ao}}{y_A}\right) + \frac{W_A}{T}(\theta_g - 1)\right\}^{-1} \tag{23}$$

$$\Theta^* = \frac{W_s^{1/h}}{\bar{\rho}_i F}\left\{\theta_g \ln\left(\frac{P^*_{Ao}}{y_A}\right) + \frac{W_A}{T}(\theta_g - 1)\right\}^{-1/h}. \tag{24}$$

The dimensionless surface area in gas-filled region of the microparticle is given by

$$S^*_{ig} = \frac{\bar{\rho}_i}{\varepsilon_i}\int_{\rho_{cp}}^{\infty} \frac{1}{\rho} f_i(\rho)\, d\rho. \tag{25}$$

The dimensionless permeability of the gas-filled region, K^*_{Pig}, and that of the liquid-filled region, K^*_{Pil}, are expressed as follows

$$K^*_{Pig} = \frac{1}{\tau_{ig}\bar{\rho}_i^2 \varepsilon_i}\int_{\rho_{cp}}^{\infty} \rho^2 f_i(\rho)\, d\rho \tag{26}$$

and

$$K^*_{Pil} = \frac{1}{\tau_{il}\bar{\rho}_i^2 \varepsilon_i}\int_0^{\rho_{cp}} \rho^2 f_i(\rho)\, d\rho \tag{27}$$

in which τ_{ig} and τ_{il} are the tortuosities in the gas-filled region and in the liquid-filled region of the microparticle, respectively. The effect of liquid-filling on τ_{ig} and τ_{il} may be more accurately captured by means of percolation and effective medium concepts; however, for the present study we use the following simple relationships:

$$\tau_{ig} = 1/\varepsilon_{ig} \tag{28}$$

$$\tau_{il} = 1/\varepsilon_{il}. \tag{29}$$

For pore volume distribution in microparticles, we assume a log-normal form:

$$f_i(\rho) = \frac{d\varepsilon_i}{d\rho} = \frac{1}{\rho\sqrt{2\pi}}\left(\frac{\varepsilon_i}{\sigma_i}\exp\left[-[\ln(\rho/\bar{\rho}_i)]^2/2\sigma_i^2\right]\right). \tag{30}$$

The energy balance within the gas-filled part includes the conduction and heat generation terms:

$$\frac{\partial^2\theta_g}{\partial x^2} + L^2\frac{\partial^2\theta_g}{\partial y^2} = -\beta\phi_o^2\left(\frac{y_A}{\theta_g}\right)^n \exp\left(\frac{\nu[\theta_g - 1]}{\theta_g}\right). \tag{31}$$

The liquid-filled region (external boundaries directly exposed to the gas): region L ($\delta(y) < x < \delta(y) + \psi$; $0 < y < 1$)

Using Darcy's law to relate the velocity and pressure gradient, the capillary driven liquid imbibition inside the pellet is given by the following equation

$$\frac{\partial^2 P^*_l}{\partial x^2} + L^2\frac{\partial^2 P^*_l}{\partial y^2} = 0. \tag{32}$$

The energy balance in the liquid phase includes contributions due to conduction as well as convection:

$$\frac{\partial^2\theta_l}{\partial x^2} + H_l\frac{\partial\theta_l}{\partial x}\frac{\partial P^*_l}{\partial x} + L^2\frac{\partial^2\theta_l}{\partial y^2} + L^2 H_l\frac{\partial\theta_l}{\partial y}\frac{\partial P^*_l}{\partial y} = 0. \tag{33}$$

The liquid-filled region (external boundaries covered by the liquid film): region LL ($\delta(y) + \psi < x < 1$; $0 < y < 1$)

The equations in this region are similar to those in region L:

$$\frac{\partial^2 P^*_{ll}}{\partial x^2} + L^2\frac{\partial^2 P^*_{ll}}{\partial y^2} = 0 \tag{34}$$

$$\frac{\partial^2\theta_{ll}}{\partial x^2} + H_l\frac{\partial\theta_{ll}}{\partial x}\frac{\partial P^*_{ll}}{\partial x} + L^2\frac{\partial^2\theta_{ll}}{\partial y^2} + L^2 H_l\frac{\partial\theta_{ll}}{\partial y}\frac{\partial P^*_{ll}}{\partial y} = 0. \tag{35}$$

The gas–liquid interface (G–L interface): ($x = \delta(y)$, $0 < y < 1$)

The G–L interface separates the completely liquid-filled region (region L) from the macropore vapor-filled region (region G). In the macropores on this surface the liquid-menisci would be situated in the interior of these pores, and their contact angle θ_c, at this dynamic equilibrium, is assumed to be same as the static equilibrium contact angle $\hat{\theta}$. Therefore, the Young–Laplace equation for mechanical equilibrium across the hemispherical shaped menisci yields

$$P^*_l = 1 - P^*_c \tag{36}$$

where, the dimensionless capillary pressure, P_c^*, is given by

$$P_c^* = \frac{2\sigma\cos(\hat{\theta})}{r_a P_o} \tag{37}$$

in which r_a is the radius of the macropores (which are assumed to be of uniform size).

The equilibrium mole fraction of A in the vapor, at the interface, is obtained by combining the Kelvin and Clausius–Clapeyron equations as

$$y_A = P_{Ao}^* \exp\left(-\frac{P_c^* C}{\theta_l} + W_A\left(1-\frac{1}{\theta_l}\right)\right). \tag{38}$$

The continuity of the net flux of component A at the interface is given by

$$\frac{D_{eA}^*}{\theta_g}\left(L\frac{\partial y_A}{\partial y}\cos(\theta) - \frac{\partial y_A}{\partial x}\sin(\theta)\right) = M_l\left(L\frac{\partial P_l^*}{\partial y}\cos(\theta) - \frac{\partial P_l^*}{\partial x}\sin(\theta)\right). \tag{39}$$

The energy balance accounting for the latent heat of vaporization yields

$$QT\left(L\frac{\partial\theta_g}{\partial y}\cos(\theta) - \frac{\partial\theta_g}{\partial x}\sin(\theta)\right) = L\frac{\partial\theta_l}{\partial y}\cos(\theta) - \frac{\partial\theta_l}{\partial x}\sin(\theta) - V\left(L\frac{\partial P_l^*}{\partial y}\cos(\theta) - \frac{\partial P_l^*}{\partial x}\sin(\theta)\right). \tag{40}$$

Further, the continuity of temperature demands that

$$\theta_g = \frac{\theta_l}{T}. \tag{41}$$

L–LL interface: ($x = \delta(y) + \psi$; $0 < y < 1$)

The continuity of energy and mass fluxes yields, respectively

$$\left(L\frac{\partial\theta_l}{\partial y}\cos(\theta) - \frac{\partial\theta_l}{\partial x}\sin(\theta)\right) = \left(L\frac{\partial\theta_{ll}}{\partial y}\cos(\theta) - \frac{\partial\theta_{ll}}{\partial x}\sin(\theta)\right) \tag{42}$$

$$\left(L\frac{\partial P_l^*}{\partial y}\cos(\theta) - \frac{\partial P_l^*}{\partial x}\sin(\theta)\right) = \left(L\frac{\partial P_{ll}^*}{\partial y}\cos(\theta) - \frac{\partial P_{ll}^*}{\partial x}\sin(\theta)\right). \tag{43}$$

In equations (39), (40), (42) and (43) above, θ is the angle at the interfacial point defined such that $\tan(\theta)$ represents the slope of the tangent to the interface [i.e. $\tan(\theta) = dY/dX = 1/L(d\delta/dy)$, where $X = \Delta(Y)$].

The boundary conditions for region G, region L and region LL are as follows:

$x = 0$; $0 < y < 1$

$$NU_{gs}(1-\theta_g) = -Q\frac{\partial\theta_g}{\partial x} \tag{44}$$

$$SH(y_{Ao} - y_A) = -\frac{D_{eA}^*}{\theta_g}\frac{\partial y_A}{\partial x} \tag{45}$$

$y = 1$; $0 < x < \delta(1)$

$$NU_{gs}(1-\theta_g) = QL\frac{\partial\theta_g}{\partial y} \tag{46}$$

$$SH(y_{Ao} - y_A) = L\frac{D_{eA}^*}{\theta_g}\frac{\partial y_A}{\partial y}. \tag{47}$$

$y = 1$; $\delta(1) < x < \delta(1) + \psi$

The external surface of the liquid-filled region (region L) is directly exposed to the bulk gas. The vapor–liquid equilibrium condition at this surface is given by

$$y_A = P_{Ao}^* \exp\left(-\frac{P_c^* \alpha C}{\theta_l} + W_A\left(1-\frac{1}{\theta_l}\right)\right) \tag{48}$$

in which

$$\alpha = \frac{\cos(\theta_c)}{\cos(\hat{\theta})}. \tag{49}$$

The macropores on this surface would be completely liquid-filled with liquid-menisci residing at the pore-mouths. Although the macropores are (assumed to be) of uniform size, the liquid menisci at the pore-mouths would acquire different curvatures in compliance with the generalized Kelvin equation [equation (1)], for different temperatures and/or partial pressures [14]. Thus, unlike the case for the gas–liquid interface which is in the interior of the pellet, for which the contact angle is assumed to be the equilibrium contact angle $\hat{\theta}$, the menisci in the macropores at the external surface can acquire a contact angle θ_c greater than $\hat{\theta}$. The condition of mechanical equilibrium of the liquid meniscus provides the additional equation for the unknown α:

$$\alpha = \frac{1 - P_l^*}{P_c^*}. \tag{50}$$

Further, the vaporization of liquid into the unsaturated surroundings is balanced by the capillary driven liquid imbibition:

$$SH(y_{Ao} - y_A) = LM_l\frac{\partial P_l^*}{\partial y}. \tag{51}$$

The energy balance at this surface includes the contributions due to conduction, the sensible heat of the imbibing liquid and the latent heat of vaporization

$$NU_{gs}(T-\theta_l) = L\left(\frac{\partial\theta_l}{\partial y} - V\frac{\partial P_l^*}{\partial y}\right). \quad (52)$$

y = 1 ; $\delta(y)+\psi < x < 1$

At this boundary the energy supplied by the intraparticle conduction and convection is removed by the external liquid film:

$$NU_{ls}(1-\theta_{ll}) = L\left(\frac{\partial\theta_{ll}}{\partial y} + H_l\frac{\partial P_{ll}^*}{\partial y}(1-\theta_{ll})\right). \quad (53)$$

The liquid phase pressure, P_{ll}, in the external liquid film is assumed to be the same as the bulk gas pressure P_o, yielding

$$P_{ll}^* = 1. \quad (54)$$

x = 1 ; 0 < y < 1

As for the previous case, the boundary conditions for this liquid covered surface are given by

$$NU_{ls}(1-\theta_{ll}) = \left(\frac{\partial\theta_{ll}}{\partial x} + H_l\frac{\partial P_{ll}^*}{\partial x}(1-\theta_{ll})\right) \quad (55)$$

and

$$P_{ll}^* = 1. \quad (56)$$

y = 0 ; 0 < x < 1

The symmetry about the x axis demands that

$$\frac{\partial y_A}{\partial y} = \frac{\partial\theta_g}{\partial y} = \frac{\partial\theta_l}{\partial y} = \frac{\partial P_l^*}{\partial y} = \frac{\partial\theta_{ll}}{\partial y} = \frac{\partial P_{ll}^*}{\partial y} = 0. \quad (57)$$

Parameters for performance evaluation

Effectiveness factor. The catalyst effectiveness factor (E_{ff}) is defined as the ratio of the observed rate to the rate of the completely utilized pellet evaluated at the bulk conditions. In dimensionless form

$$E_{ff} = \frac{M_l}{\phi_o^2 y_{Ao}^n}\left\{\int_0^1\left(\frac{\partial P_{ll}^*}{\partial x}\right)_{x=1}\mathrm{d}y + \int_{\delta(1)+\psi}^1 L^2\left(\frac{\partial P_{ll}^*}{\partial y}\right)_{y=1}\mathrm{d}x + \int_{\delta(1)}^{\delta(1)+\psi} L^2\left(\frac{\partial P_l^*}{\partial y}\right)_{y=1}\mathrm{d}x\right\}$$
$$+ \frac{1}{\phi_o^2 y_{Ao}^n}\left\{\int_0^{\delta(1)} L^2\left(\frac{D_{eA}^*}{\theta_g}\frac{\partial y_A}{\partial y}\right)_{y=1}\mathrm{d}x - \int_0^1\left(\frac{D_{eA}^*}{\theta_g}\frac{\partial y_A}{\partial x}\right)_{x=0}\mathrm{d}y\right\}. \quad (58)$$

Wetting efficiencies. The external wetting efficiency (η_{ex}) is defined as the fraction of the external area of the pellet covered by the liquid film:

$$\eta_{ex} = \frac{1+L\gamma}{2+L}. \quad (59)$$

The internal wetting efficiency (η_i) is defined as the fraction of total volume of the pellet completely filled by liquid:

$$\eta_i = 1 - \int_0^1 \delta(y)\,\mathrm{d}y. \quad (60)$$

NUMERICAL SOLUTION

Coordinate transformation

The problem is fully defined by the model equations (15)–(57). The numerical solution of this coupled set of equations in y_A, θ_g, θ_l, P_l^*, θ_{ll} and P_{ll}^* is complicated by the fact that the position and shape of the gas–liquid interface is unknown. Consequently, the approach used here is to simplify the numerical analysis by transforming the nonorthogonal free boundary (G–L interface) to an orthogonal fixed boundary at the expense of complicating the governing partial differential equations [25]. The following transformations are used for this purpose:

In region G ($0 \leqslant x \leqslant \delta(y)$, $0 \leqslant y \leqslant 1$)

$$x_g = \frac{x}{\delta(y)}, \quad y \text{ unchanged} \quad (61)$$

In region L ($\delta(y) \leqslant x \leqslant \delta(y)+\psi$, $0 \leqslant y \leqslant 1$)

$$x_l = \frac{x-\delta(y)}{\psi}, \quad y \text{ unchanged.} \quad (62)$$

In region LL ($\delta(y)+\psi \leqslant x \leqslant 1$, $0 \leqslant y < 1$)

$$x_{ll} = \frac{x-(\delta(y)+\psi)}{1-(\delta(y)+\psi)}, \quad y \text{ unchanged.} \quad (63)$$

Solution methodology

The general methodology used to solve the transformed equations is as follows. By fixing the interface position, the combined set of field equations in various regions and boundary conditions is discretized, using two-dimensional orthogonal collocation [26], and solved to obtain the profiles of θ_g, y_A, θ_l, θ_{ll}, P_l^* and P_{ll}^*. These are then used to evaluate the residuals of the discretized energy balance equations at the interface, which are then used to obtain an improved interface position and iteratively reduced. All integrals were evaluated by Gauss–Legendre quadrature, and the system of nonlinear equations resulting from the discretization was solved using a Marquardt–Levenberg method. Numerical experiments indicated that a 3×3 square grid of interior collocation points in each region was adequate. For iterative searching of the interface position, pseudo-transient energy balance equations were formulated with residuals representing the false accumulation terms written as $w_i\,\mathrm{d}\delta_i/\mathrm{d}t$. Here the w_is are weight factors chosen by trial and error to accelerate the convergence. The system of pseudo-transient equations at the interface points is integrated using Gear's method, with the accumulation terms becoming negligible as the true interface position is approached.

Table 1. Base-case parameter values

Geometric and structural parameters	
$L = 4.0$	$\sigma_i = 0.2$
$\gamma = 0.15$	$\bar{p}_i = 0.1$
$\varepsilon_a = 0.3$	$d_{AK} = 0.55$
$\varepsilon_i = 0.5$	
Kinetic parameters	
$\nu = 10.0$	ϕ_o = variable
$\beta = 0.05$	
Thermodynamic parameters	
$P_c^* = 5.0$	$W_A = 12.0$
$P_{Ao}^* = 0.1$	$W_S = 3.0$
$T = 1.0$	$F = 75$
$C = 0.004$	$h = 1.5$
Transport parameters	
$V = 0.01$	$y_{Ao} = 0.06$
$H_l = 0.035$	$NU_{gs} = 0.7$
$M_l = 0.4$	$NU_{ls} = 1.0$
$Q = 1.0$	$SH = 100.0$

RESULTS AND DISCUSSION

The base-case parameter values used for the numerical study are listed in Table 1. These parameters are evaluated for a typical realistic case at atmospheric pressure. Parameters other than those whose values are indicated on the figures that follow assume the values indicated in Table 1.

Transport of condensable component in the vapor-filled region

Since the observed rate of reaction in a catalyst particle is strongly influenced by intraparticle mass transfer, surface and capillary condensate transport may be expected to play a significant role in vapor phase reactions carried out at temperatures near the boiling point of reactants or products [27]. The representation of these phenomena in the catalyst pellet is therefore a unique feature of this study, hitherto not considered. Figure 2(a) shows the variation of dimensionless microparticle diffusivity with relative saturation of the gas phase, predicted for the base-case parameters used in this work. Indeed, the reported slight fall in diffusivity in the multilayer region followed by the anomalous rise, at higher relative saturation, in the capillary condensation region [28] are well represented by the model. Further, as seen in Fig. 2(b) and (c), the model also predicts adsorption–desorption hysteresis similar to that observed [28, 29], and also the maximum in diffusivity as saturation is approached, reported by some workers [28, 30, 31]. Of particular significance is the strong influence of micropore size distribution, seen in Fig. 2(a), and the several-fold enhancement in effective pellet diffusivity over the normal (nonadsorbable) gas phase value [cf. Fig. 2(c)], due to the higher rate of transport in the microparticles. The detailed explanations for these trends, including the peculiar maxima in Fig. 2(a)–(c), are provided elsewhere [18].

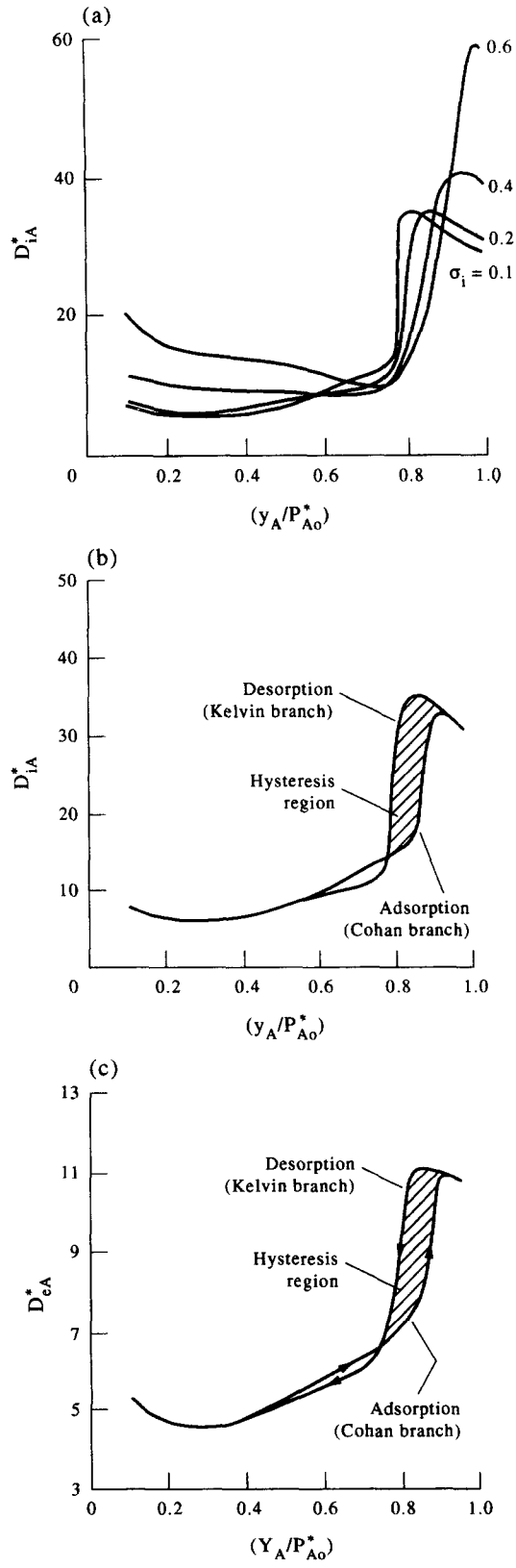

Fig. 2. Variation of dimensionless diffusivity with relative saturation, at $\theta_g = 1$. (a) Kelvin branch in microparticle, for various values of σ_i, (b) hysteresis in microparticle and (c) hysteresis in pellet.

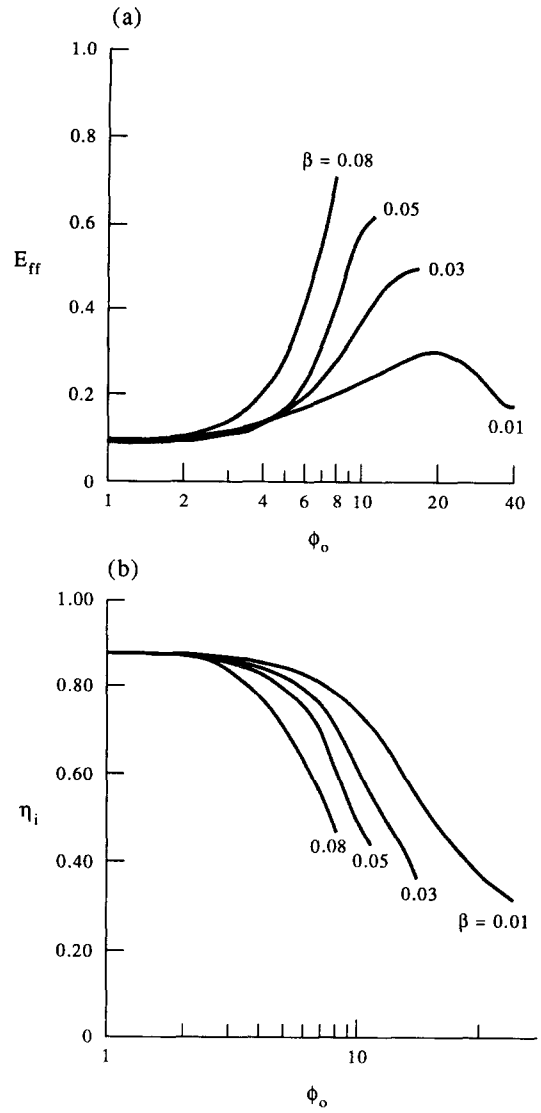

Fig. 3. Effect of β on the Thiele modulus (ϕ_0) dependence of (a) effectiveness factor (E_{ff}) and (b) internal wetting efficiency (η_i).

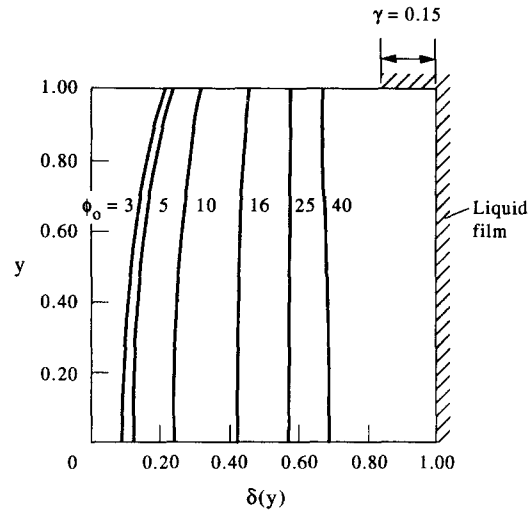

Fig. 4. Position of G–L interface for various values of Thiele modulus (ϕ_0) and $\beta = 0.01$.

Steady state behavior of the catalyst pellet

Since a large number of parameters are involved only the role of the key parameters is reported here. Further, only stable steady states are reported as the pseudo-transient solution strategy did not permit attainment of unstable steady states. Also, the numerical solution method was most effective for states with internal wetting between 40 and 90%, with solutions corresponding to mostly dry states not being attained. This, however, is a reasonably wide range essentially covering the region of practical interest. As usual the performance of the catalyst pellet is represented by the effectiveness factor (E_{ff}), which is a net result of the sensitive balance between the different phenomena occurring in the various regions of the two-dimensional pellet.

Effect of β. Figure 3(a) and (b) shows the impact of the dimensionless heat of reaction (Prater number β) on the dependence of effectiveness factor (E_{ff}), and of internal wetting efficiency (η_i), on the Thiele modulus (ϕ_o). It may be anticipated that for sufficiently small ϕ_o values (i.e. low reaction rate) the impact of the dimensionless heat of reaction, β, is negligible, and E_{ff} and η_i approach constant values independent of β. This is evident in Fig. 3(a) and (b), and the influence of β becomes more significant at smaller ϕ_o values for larger values of β. With further increase in ϕ_o the rate of reaction becomes increasingly sensitive to ϕ_o, and for sufficiently large β [$\beta = 0.08$, in Fig. 3(a)] the reaction heat exceeds the demands of the latent heat for vaporization, causing net heating of the pellet, thereby raising the saturation vapor pressure at the interface. The increased supply of the condensable reactant from the interface and the higher temperature further intensifies the reaction rate, and this may lead to 'reaction run-away' and eventually to a 'hot-spot'.

For smaller values of β [$\beta = 0.01$, in Fig. 3(a)] the reaction heat is not sufficient to overcome the cooling caused by vaporization, and the initial increase in E_{ff} with ϕ_o is mainly due to the increase in gas-filled volume (in which the reaction occurs) caused by the higher vaporization rate accompanying the higher reaction rate. The intra-pellet diffusion time increases as the gas-filled portion penetrates further inside the pellet. Further, the higher intrinsic rate at higher ϕ_o leads to the depletion of A in the interior of the pellet and, as y_A decreases, the liquid-filled pores in the microparticles in the vapor-filled region start opening up, reducing the effective diffusivity. Consequently, at high ϕ_o the overall reaction rate is controlled by intrapellet diffusion, indicated by the descending portion of E_{ff} vs ϕ_o curve, for $\beta = 0.01$.

Shape of the interface. Figure 4 shows the location and shape of the interface at different ϕ_o values, corresponding to $\beta = 0.01$ in Fig. 3. At low ϕ_o the vaporization is mainly due to the existence of unsaturated surroundings, and occurs more near the faces of

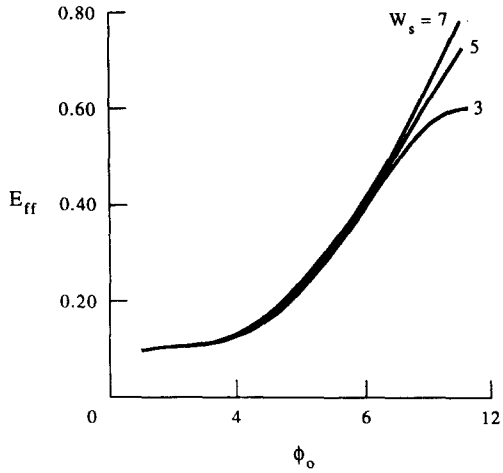

Fig. 5. Variation of effectiveness factor (E_{ff}) with Thiele modulus (ϕ_0) for various values of W_s and $\beta = 0.05$.

the pellet than in the interior, where the additional intrapellet diffusion resistance becomes important. Both of these factors lead to the convex shape at low ϕ_o. With increasing ϕ_o the gradient of mole fraction y_A becomes steeper leading to increased vaporization in the interior of the pellet, and therefore to flattening of the interface. At very high ϕ_o values the reactant (A) is almost completely consumed within the pellet and the interface shape becomes slightly concave. In this situation the pellet is starved of condensable component A which consequently also diffuses into the pellet from the unsaturated surroundings.

Effect of W_s. As discussed above, for intermediate values of β (e.g. $\beta = 0.05$, in Fig. 3) and high ϕ_o, in the vapor filled region the rate is governed by intrapellet diffusion and y_A is low. In this condition most of the vapor-filled region is devoid of capillary condensate and the transport is mainly due to surface diffusion through the microparticles. Figure 5 shows the E_{ff} vs ϕ_o plot for $\beta = 0.05$, for different values of the extent-of-adsorption-related parameter W_s. Other parameters remaining unchanged, a higher W_s implies greater extent of adsorption (that is greater Θ^*), and hence higher D_{iA}^{s*} [equations (18) and (24)]. Thus, the effect of W_s is more prominent at high ϕ_o where surface diffusion is more important. At lower ϕ_o, where the pellet is colder, transport in the vapor-filled region is dominated by capillary condensate transport in the microparticles, and the curves for different W_s in Fig. 5 merge into each other.

Effect of SH. Figure 6(a) and (b) shows the effect of Sherwood number, SH, on the variation of E_{ff} with Thiele modulus ϕ_o, for two different values of the parameter V (which signifies the relative importance of phase change-related heat transfer to conductive heat transfer in the liquid phase). At low ϕ_o incomplete internal wetting, despite the negligible reaction heat effects, is due to the surroundings being unsaturated. With increase in the Sherwood number the transport of condensable component A into the surroundings increases, and hence the internal wetting decreases. Larger V prevents vaporization by cooling of the liquid front, thereby reducing the saturation vapor pressure and hence the driving force for vapor transport. Thus, for $V = 0.01$ (base-case value), the cooling effect due to latent heat removal is much more significant than that for $V = 0.002$. For $SH = 40$ and 50 and $V = 0.01$, in Fig. 6(a), a 'completely established' interface (that is, the interface located away from the $x = 0$ face of the pellet) does not exist for low ϕ_o values. The numbers in brackets in Fig. 6(a) and (b), indicate the extent of internal wetting for the corresponding values of ϕ_o. For $SH = 40$ and $V = 0.01$ [Fig. 6(a)] $\phi_o = 8$ represents the 'extinction point', for on slight reduction of ϕ_o thermal instability sets in, and the pellet is almost completely filled with

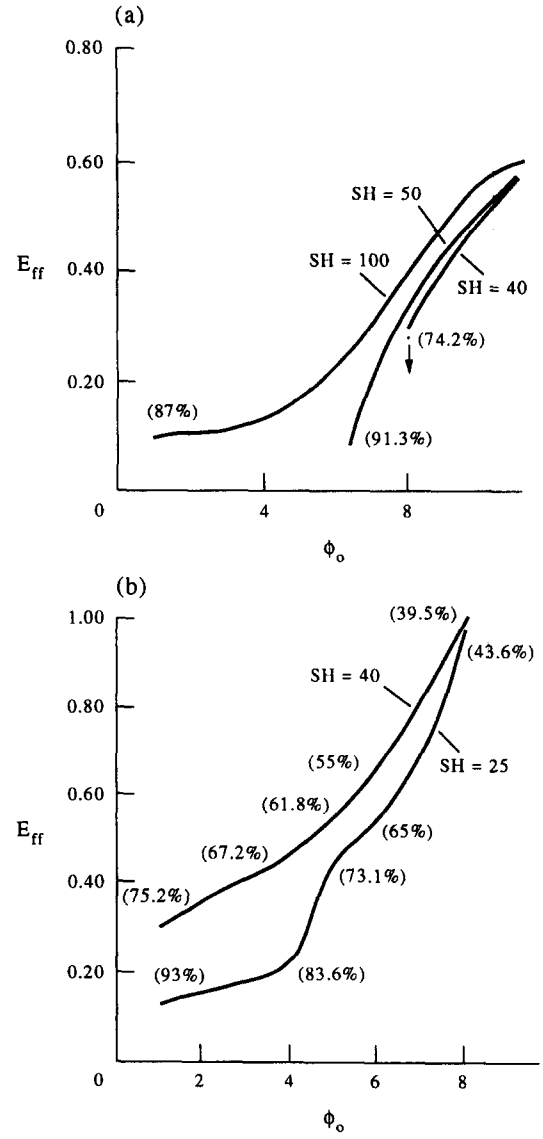

Fig. 6. Variation of effectiveness factor (E_{ff}) with Thiele modulus (ϕ_0), for various values of SH and (a) $V = 0.01$, (b) $V = 0.002$. Numbers in parentheses indicate the internal wetting efficiency.

liquid. On the other hand, because of smaller cooling effects at lower V [$V = 0.002$, Fig. 6(b)] a completely established interface is possible, even for $SH = 25$ and $\phi_o = 1$.

The unusual trend for $SH = 25$ in Fig. 6(b) can be explained as follows. At low ϕ_o, because of the smaller gas-filled volume available for reaction, evaporation due to reaction heat effects is delayed up to $\phi_o = 4.0$, so that the effectiveness factor is only weakly sensitive to ϕ_o. As ϕ_o increases the gas filled volume gradually increases, and the intrinsic reaction rate becomes increasingly sensitive to ϕ_o. Beyond $\phi_o = 4$, the temperature starts rising and rapid evaporation ensues. However, as temperature rises the capillary held liquid in the microparticles in the vapor-filled region (region G) starts vaporizing, and the effective diffusivity decreases. This slightly retards the rate, explaining the slight deviation from the normal trend in the range $\phi_o = 4$–6. Beyond $\phi_o = 6$, however, the reaction rate and internal temperature as well as evaporation rate increase rapidly, and E_{ff} is again more sensitive to ϕ_o.

Effect of M_l. The parameter M_l represents the ratio of the resistance to transport in vapor filled pores to that in liquid filled pores. At low ϕ_o it may be anticipated that the internal wetting (η_l) is greater for larger values of M_l, so that the smaller gas filled volume available for reaction results in smaller E_{ff}. Further, for smaller M_l the external mass transfer resistance becomes less important as compared to the resistance for the imbibition transport of liquid on the surface of region L [equation (51)]. Hence, for sufficiently small M_l, the evaporation is controlled by the slower imbibition of liquid, and the liquid in the pore-mouths attains thermodynamic equilibrium with the bulk gas. Thus, y_A near the external surface of region L is smaller for smaller value of M_l and so is the equilibrium temperature of the liquid in the pore-mouths. Because of this restriction, the temperature and the saturation vapor pressure at the interface are smaller for smaller M_l. Furthermore, the smaller the M_l the smaller is the dimensionless effective diffusivity D^*_{cA} [equations (17)–(19)]. For these reasons, as discussed before [for $\beta = 0.01$ in Fig. 3(a)], at higher ϕ_o and sufficiently small M_l, the overall reaction rate is controlled by the intrapellet diffusion process, which is evident from the descending portion of the E_{ff} vs ϕ_o curve in Fig. 7 for $M_l = 0.05$. On the other hand, for larger M_l the restriction mentioned above is less severe, and the interface can attain higher temperatures at larger ϕ_o, so that greater saturation vapor pressures and higher effective diffusivities result in larger E_{ff}.

Effect of external wetting efficiency. Figure 8 shows the effect of dimensionless capillary pressure P^*_c on the variation of effectiveness factor with the external wetting efficiency-related parameter γ [cf. equation (59)], for $\phi_o = 6$. Larger P^*_c implies greater wettability of the pore structure due to greater driving force for imbibition, and also due to enhanced capillary condensation caused by the reduced vapor pressure.

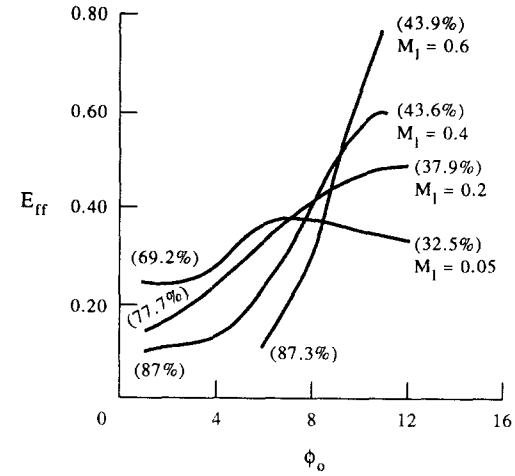

Fig. 7. Variation of effectiveness factor (E_{ff}) with Thiele modulus (ϕ_0) for various values of M_l. Numbers in parentheses indicate the internal wetting efficiency.

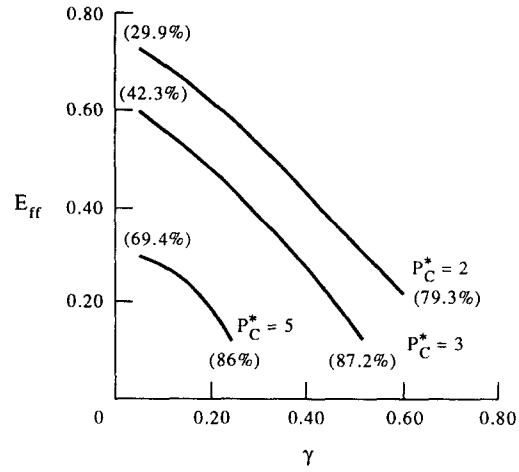

Fig. 8. Variation of effectiveness factor (E_{ff}) with dimensionless length of liquid film in x direction (γ), for various values of P^*_c and $\phi_0 = 6$. Numbers in parentheses indicate the internal wetting efficiency.

Consequently, at constant γ, the effectiveness factor factor decreases with increase in P^*_c, due to the attendant decrease in the vapor-filled space which dominates the rate. Also, as expected, for a fixed P^*_c, as γ increases the gas-filled volume decreases due to increased imbibition from the liquid covered portion of the pellet, and hence the effectiveness factor decreases. Such an effect has been reported [32], but prior analyses considering only liquid-filled pores, in spite of evidence to the contrary [32], could not associate this with the partial internal wetting.

REFERENCES

1. G. A. Funk, M. P. Harold and K. M. Ng, A novel model for reaction in trickle-beds with flow maldistribution, *Ind. Engng. Chem. Res.* **29**, 738–748 (1990).
2. D. H. Kim and Y. G. Kim, An experimental study of multiple steady-states in a porous catalyst due to phase transition, *J. Chem. Engng Japan* **14**, 311–317 (1981).

3. D. H. Kim and Y. G. Kim, Simulation of multiple steady-states in a porous catalyst due to phase transition, *J. Chem. Engng Japan* **14,** 318–322 (1981).
4. S. K. Bhatia, Steady-state multiplicity and partial internal wetting of catalyst particles, *A.I.Ch.E. Jl* **34,** 969–979 (1988).
5. S. K. Bhatia, Partial internal wetting of catalyst particles with a distribution of pore size, *A.I.Ch.E. Jl* **35,** 1337–1345 (1989).
6. D. N. Jaguste and S. K. Bhatia, Partial internal wetting of catalyst particles: hysteresis effects, *A.I.Ch.E. Jl* **37,** 650–660 (1991).
7. I. V. Yentekakis and C. G. Vayenas, Effectiveness factors for reactions between volatile and nonvolatile components in partially wetted catalysts, *Chem. Engng Sci.* **42,** 1323–1332 (1987).
8. C. S. Tan, Effectiveness factors of *n*-th order reactions for incomplete wetting of particles in trickle-bed reactors, *Chem. Engng Sci.* **43,** 1281–1286 (1988).
9. W. Sedriks and C. N. Kenney, Partial wetting in trickle-bed reactors—the reduction of crotonaldehyde over a palladium catalyst, *Chem. Engng Sci.* **28,** 559–568 (1973).
10. O. M. Martinez, G. F. Barreto and N. O. Lemcoff, Effectiveness factor of a catalyst pellet in a trickle bed reactor—limiting reactant in the gas phase, *Chem. Engng Sci.* **36,** 901–907 (1981).
11. W. Sakornwimon and N. D. Sylvester, Effectiveness factors for partially wetted catalysts in trickle-bed reactors, *Ind. Engng Chem. Process. Des. Dev.* **21,** 16–25 (1982).
12. M. P. Harold, Steady-state behavior of the non-isothermal partially wetted and filled catalyst, *Chem. Engng Sci.* **43,** 3197–3216 (1988).
13. D. N. Miller and R. S. Kirk, Kinetics of catalytic dehydration of primary alcohols, *A.I.Ch.E. Jl* **8,** 183–189 (1962).
14. D. H. Everett and J. M. Haynes, Model studies of capillary condensation—I. Cylindrical pore model with zero contact angle, *J. Colloid Interface Sci.* **38,** 125–137 (1972).
15. R. Defay and I. Prigogine, *Surface Tension and Adsorption*, Chaps. 1 and 15. Longman, London (1966).
16. D. M. Young and A. D. Crowell, *Physical Adsorption of Gases*, p. 169. Butterworths, London (1962).
17. M. M. Qui and S-T. Hwang, Continuous vapor–gas separation with a porous membrane permeation system, *J. Membrane Sci.* **59,** 53–72 (1991).
18. D. N. Jaguste and S. K. Bhatia, *Chem. Engng Sci.* accepted.
19. E. A. Flood, R. H. Tomlinson and A. E. Leger, The flow of fluids through activated carbon rods: the flow of adsorbed fluids, *Can. J. Chem.* **30,** 348 (1952).
20. H. Tsujikawa, T. Osawa and H. Inoue, Separation of benzene and nitrogen through porous vycor glass, *Int. Chem. Engng* **27,** 479–487 (1987).
21. J. C. Maxwell, *Electricity and Magnetism*, pp. 435–445. Clarendon Press, Oxford (1892).
22. K. A. Akanni, J. W. Evans and I. S. Abramson, Effective transport coefficients in heterogeneous media, *Chem. Engng Sci.* **42,** 1945–1954 (1987).
23. J. J. Sangiovanni and A. S. Kesten, Analysis of gas pressure build up within a porous catalyst particle which is wet by a liquid reactant, *Chem. Engng Sci.* **26,** 533–547 (1971).
24. C. N. Satterfield and F. Ozel, Direction solid catalysed reaction of a vapor in an apparently completely wetted trickle bed reactor, *A.I.Ch.E. Jl* **19,** 1259–1261 (1973).
25. J. Crank, *Free and Moving Boundary Problems*, Chap. 5. Clarendon Press, Oxford (1984).
26. B. A. Finlayson, *Non-Linear Analysis in Chemical Engineering*, Chap. 6. McGraw-Hill, New York (1980).
27. A. Wheeler, *Advances in Catalysis*, Vol. 3, p. 274. Academic Press, New York (1951).
28. K.-H. Lee and S.-T. Hwang, The transport of condensible vapors through a microporous vycor glass membrane, *J. Colloid Interface Sci.* **110,** 544–555 (1986).
29. J. M. Haynes and R. J. Miller, In *Adsorption at the Gas–Solid and Liquid–Solid Interface* (Edited by J. Rouquerol and K. S. W. Sing), pp. 439–447. Elsevier Scientific, Amsterdam (1982).
30. P. E. Eberly and D. B. Vosberg, Diffusion of benzene and inert gases through porous media at elevated temperatures and pressures, *Trans. Faraday Soc.* **61,** 2724–2735 (1965).
31. K. Kammermeyer, Gaseous diffusion through microporous and adsorbent membranes, *Chem. Engng Prog. Symp. Ser.* **55,** 115–125 (1959).
32. C. N. Satterfield, Trickle bed reactors, *A.I.Ch.E. Jl* **21,** 209–228 (1975).